K-shell spectroscopy of an independently diagnosed uniaxially expanding laser-produced aluminum plasma

D. M. Chambers* and P. A. Pinto
Steward Observatory, University of Arizona, Tucson, Arizona 85721

J. Hawreliak, I. R. Al'Miev, A. Gouveia, P. Sondhauss, E. Wolfrum,[†] and J. S. Wark
Department of Physics, Clarendon Laboratory, University of Oxford, Oxford, OX1 3PU, United Kingdom

S. H. Glenzer, R. W. Lee, and P. E. Young
Lawrence Livermore National Laboratory, University of California, P.O. Box 808, Livermore, California 94551

O. Renner
Institute of Physics, Czech Academy of Sciences, 18221 Prague, Czech Republic

R. S. Marjoribanks
Department of Physics, McLennan Physical Laboratories, University of Toronto, Toronto, Ontario, Canada M5S 1A7

S. Topping
School of Mathematics and Physics, Queens University Belfast, Belfast BT7 1NN, United Kingdom

We present detailed spectroscopic analysis of the primary *K*-shell emission lines from a uniaxially expanding laser-produced hydrogenic and heliumlike aluminum plasma. The spectroscopic measurements are found to be consistent with time-dependent hydrodynamic properties of the plasma, measured using Thomson scattering and shadowgraphy. The *K*-shell population kinetics code FLY with the measured hydrodynamic parameters is used to generate spectra that are compared to the experimental spectra. Excellent agreement is found between the measured and calculated spectra for a variety of experimental target widths employed to produce plasmas with different optical depths. The peak emission from the hydrogenic Lyman series is determined to be from a temporal and spatial region where the hydrodynamic parameters are essentially constant. This allows a single steady-state solution of FLY to be used to deduce the electron temperature and density, from the measured line ratios and linewidths, for comparison with the Thomson and shadowgraphy data. These measurements are found to agree well with time-dependent calculations, and provide further validation for the FLY calculations of the ionization and excitation balance for a *K*-shell aluminum plasma. We also discuss the possible application of this data as a benchmark for hydrodynamic simulations and ionization/excitation balance calculations.

I. INTRODUCTION

Detailed understanding and modeling of the x-ray line emission from laser-produced plasmas is a complex process even for *K*-shell spectra. Laser-produced plasmas exhibit large gradients in density, temperature, and velocity, all of which have considerable influence on the spectra received by a distant observer [1–5]. Over the past few years considerable effort has been expended to measure at high spectral resolution, and subsequently to model, the resonance line emission from laser-produced hydrogenic aluminum plasmas [6–10]. These studies have largely been made possible by the development of novel forms of high-resolution x-ray spectrometers, providing both high spectral and spatial resolution [11,12]. It has been shown that the velocity gradient

within the plasma plays a prominent role in determining both the line shape of the emitted radiation, as well as its intensity. Reasonably good agreement has been found between experimental and modeled spectra, with the absolute photon numbers observed agreeing to within 50%, and observed line shapes (recorded at high resolution) being well matched, at least in terms of the gross features, by models that take into account plasma gradients in the radiation transfer calculations [10].

However, although reasonable agreement was obtained, it should be stressed that the hydrodynamic parameters used in the modeling of the x-ray spectra in the work cited above came solely from the hydrocodes: no independent measurements (that is to say, independent of the x-ray spectra themselves) of the densities, temperatures, and velocities present within the plasma were recorded. Indeed, to our knowledge, there is a dearth of experimental spectroscopic data where detailed hydrodynamic information has been obtained by means independent of the spectroscopy. Thus, in order to fully understand the effects of the inhomogeneity of the plasma on the observed x-ray emission, it is of great impor-
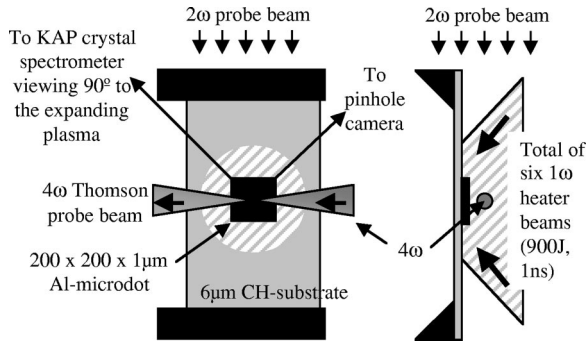
FIG. 1. The experimental target geometry, showing the directions to the various diagnostics and probe beams.

tance to measure accurately and independently the hydrodynamic parameters of the plasma in question as well as its spectral emission. Only if both types of measurement are consistent can we begin, with confidence, to claim to have a good understanding of the overall emission from such plasmas. To this end, we present detailed K-shell spectroscopic measurements of an expanding laser-produced aluminum plasma. In this paper we will concentrate on analyzing the ratios and intensities of the K-shell spectra, and the line shapes inasmuch as they yield density information. We leave the effects of the velocity gradient on the emergent spectrum of the Ly-α radiation for a future publication. Independent measurements are presented of the electron temperature and density, using Thomson scattering and shadowgraphy. In order to simplify the analysis of these measurements we have utilized the so-called ''dot targets,'' described in more detail below, that form plasmas which exhibit expansion along one axis only. The majority of the spectral measurements are then taken perpendicular to, and spatially resolved along, the plasma expansion direction.

Various spectroscopic measurements and simulations have been used for over 20 years to gain information on the hydrodynamic conditions and ionization balance of laser-produced plasmas; for example, see Refs. [13–21]. However, there have been few previous attempts to benchmark hydrodynamic simulations or ionization balance calculations [22–24] and, to our knowledge, no complete experimental benchmark data set exists. A one-dimensional plasma expansion provides an ideal experimental environment to compare with current hydrodynamic simulations. Thomson scattering provides an accurate noninvasive method to measure the hydrodynamic parameters of laser-produced plasmas [24–26]. The features of the Thomson scattered signal can, in principle, provide the electron temperature, electron density, plasma velocity, average ionization stage ($\bar{Z}$), and by inference the ion temperature, density, and even information on the heat flow. A one-dimensional plasma, diagnosed by spatially and temporally resolved Thomson scattering, would therefore provide an appropriate benchmark for any hydrodynamic simulation. Further, when the Thomson scattering measurements are coupled with high-resolution spectroscopy, we have a method to benchmark calculations of the x-ray spectra that is sensitive to the ionization and excitation balance. Whilst providing a complete benchmark for simulations and

ionization balance calculations is beyond the scope of the current paper, we will revisit this idea in the conclusions and identify where the current data we present here needs to be augmented and/or improved upon.

It is also of interest to note that the types of experiments described here may also have some relevance to several astrophysical situations, where several phenomena have strong velocity gradients which considerably affect their emitted spectra. Though on a completely different spatial and temporal scale, the basic physics behind the radiation transfer process is essentially the same. A well diagnosed laboratory experiment could therefore provide a simple test case for simulations used to diagnose astrophysical events such as supernovas or accretion disks.

II. EXPERIMENTAL ARRANGEMENT

The experiments were performed using the Vulcan laser facility [27], at the Rutherford Appleton Laboratory, UK. Six beams of the Vulcan laser were focused using $f/10$ lenses onto an aluminum microdot target mounted onto a plastic (parylene-n, C_8H_8) foil, see Fig. 1. Each beam provided ~ 150 J at 1.053 μm in a 1.1 ns (full width at half maximum, FWHM) flat topped trapezoidal pulse shape with 150 ps rise and fall times. Random phase plates ensured each beam provided a uniform intensity profile across the target into a 500 μm diameter focal spot. This produced an intensity on target of 3.5×10^{14} W cm^{-2} for the 950 ps duration of the peak of the pulse. The aluminum microdot was 1 μm thick, 200 μm high, ranged between 50 and 400 μm wide, and centrally positioned within the laser foci. This overillumination of the microdot ensured a one-dimensional aluminum plasma expansion, as the aluminum plasma was confined by expanding CH plasma on all sides. The CH foil was 1 mm wide and 6 μm thick and was mounted between two metallic jaws 3 mm apart.

Two additional beams of the Vulcan laser were used to probe the plasma conditions. The first was frequency quadrupled and focused into the expanding plasma at 90° to the expansion direction using an $f/10$ lens. This beam provided up to 50 J in a 2 ns trapezoidal pulse, and was timed to begin with the main six heater pulses. The Thomson scattered light from this beam was collected in the direction of plasma expansion using an $f/10$ lens, relay imaged into a 1 m Spex spectrometer incorporating a 3600l/mm grating, and collected using an Imacon 500 streak camera. This ensured that the ion feature of the Thomson scattering spectrum was resolved at all times during the 2 ns probe laser pulse. The second 2 ns probe beam was frequency doubled and a collimated 1 cm section passed over the target at 90° to both the plasma expansion and the Thomson scattering probe beam. The shadow of the plasma in this beam was imaged onto a Kentech gated optical imager. Three separate cameras took 100 ps gated images at 0.5, 1.0, and 1.5 ns after the start of the laser pulses. The magnification of the imaging system was ~ 10 and provided a spatial resolution to the images of ~ 10 μm. Two pinhole cameras monitored the aluminum plasma hard x-ray emission ($\geqslant 1$ keV) on each shot onto 8 bit Pulnix charge-coupled device (CCD) cameras. No emis-

sion from the CH plasma registered on these devices. One camera monitored the emission from the front of the target, and the other from $90°$ to the plasma expansion direction. The magnification of these cameras varied between 2 and 4 and provided a spatial resolution of ~ 15 μm limited by the $10–12.5$ μm pinhole apertures. These cameras provided an online diagnostic on the aluminum plasma emission uniformity, and were used to identify any deviation from a one-dimensional expansion in terms of lateral expansion of the aluminum plasma on any axis.

The bulk of the spectroscopic measurements were made with a single crystal spectrometer (SCS), positioned at $90°$ to the target normal, incorporating a 15 μm entrance slit and a potassium hydrogen phthalate (KAP) crystal cleaved on the (100) plane. An Andor 16 bit x-ray CCD camera was used to detect the images. This spectrometer recorded a wavelength range between 5.4 and 6.8 Å, encompassing six primary aluminum *K*-shell lines, namely, Ly-β, Ly-γ, Ly-δ, He-β, He-γ, and He-δ. In this paper we take the following notation for the *K*-shell emission lines; we use Ly- to denote the hydrogenic aluminum Lyman series ($1s$-np, where n is the upper energy level), and He- to denote the helium-like aluminum ($1s^2$-$1snp$) principal series transitions. The spectral resolution was limited by source broadening to between 20–40 mÅ, depending on the size of the aluminum microdot. This spectrometer also spatially resolved and magnified ($\times 3$) the spectra in the plasma expansion direction with a resolution of ~ 20 μm. A vertical dispersion variant Johann crystal spectrometer (VJS) [12] was also used, utilizing a cylindrically bent quartz crystal (100), and the images recorded on direct exposure x-ray film. This spectrometer resolved individual Lyman series spectral line profiles on each shot ranging from Ly-α to Ly-η ($n=1$–2 to $n=1$–8 transitions) with a resolution of ~ 0.85 mÅ. This device was also positioned at $90°$ to the target normal, and had a spatial resolution of ~ 10 μm in the plasma expansion direction.

In addition to these diagnostics two vertical variant double crystal spectrometers (DCV's) [11] were used to measure the Ly-α emission for a variety of different emission angles from the plasma. The DCV's provided a spectral resolution of ~ 0.8 mÅ, partially limited by the 200 μm height of the aluminum microdots, and a spatial resolution of ~ 10 μm. The measurements at angles other than $90°$ to the target normal will not be discussed further here, but will provide the basis for future work to analyze the effect of the velocity gradient, and as a possible benchmark for radiation transfer simulations.

III. DENSITY AND TEMPERATURE MEASUREMENTS

As we have outlined above, we wish to have measurements of the temperature and density of the plasma that are independent of the spectroscopy. These parameters may then be used as the basis for producing synthetic spectra to compare with the experimental data. Ideally, such independent hydrodynamic information would allow us to make comparisons between modeled and experimental spectra without making recourse to hydrodynamic simulations.

In the work we present here, we obtained information about the electron temperature, plasma velocity, and electron density by use of a combination of Thomson scattering and shadowgraphy. The methods of collection and analysis of these data have been discussed in previous publications [28,29], and thus we will not go into detail here, and provide information sufficient only for the sake of clarity and completeness.

Electron temperature measurements were obtained by means of time-resolved Thomson scattering, as described in Sec. II. For each target shot the Thomson beam interrogated a volume of dimensions roughly $50 \times 50 \times 100$ μm, at a distance from the target surface that could be varied anywhere between 50 and 500 μm on each shot. The electron temperature as a function of time was deduced from the shape and separation of the ion-acoustic peaks, as outlined in Ref. [29]. We estimate that the Thomson scattering diagnostic provided temporally resolved electron temperatures with an accuracy of order $\pm 10\%$—the error being mainly due to uncertainties in the electron density and ionization level of the plasma.

The spectrometer recording the Thomson spectrum was a high-resolution, low-spectral coverage instrument. It thus only recorded the narrow spectral features of the Thomson spectrum produced by scattering from ion-acoustic waves. The electron density, which can be inferred from the broad spectral features produced by scattering from electron-plasma waves, was therefore not obtained from this measurement. In order to provide further independent information concerning the electron density, the plasma was also interrogated by shadowgraphy, as described in Ref. [28]. Shadowgraphy does not explicitly provide density information; but gives information on the combination of the density and density gradient at the edge of the shadowed region. For each target probed, a series of 100 ps snapshot images were taken showing the temporal expansion of the plasma region through which the 527 nm probe beam either could not pass, or was refracted sufficiently that it was not collected by the imaging system. To infer density information we simulate the experiments using the one-dimensional Lagrangian hydrocode MEDUSA [30,31]. We find that the simulated density and density gradients are consistent with the measured spatial extent of the shadow cast by the expanding aluminum/CH plasma. It should be noted, however, that the spatial extent of the measured shadow region from the target surface was between 0.5 and 1.5 mm, somewhat farther than the distances from which the spectral data was taken. We thus have some degree of confidence that the densities predicted by the hydrocode are trustworthy. Therefore, although we shall from this point on take densities predicted from the hydrocode as input to our spectral calculations (as opposed to the temperatures, which can be deduced directly from the Thomson spectra) it should be borne in mind that the code predictions are consistent with the independent shadowgraphy data. Furthermore, as we shall see in Sec. IX, the simulated densities close to the target surface are consistent with measurements of the Stark widths of the Lyman β and δ spectral lines.

It is also important to note at this juncture that the temperatures predicted by MEDUSA at distances greater than
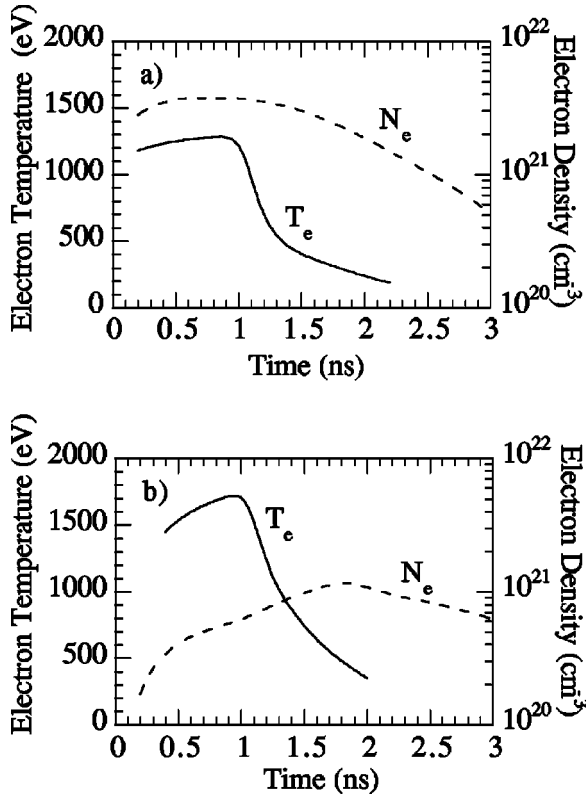
FIG. 2. Electron temperatures (solid line) and electron densities (dashes) as a function of time at 50 (a) and 300 (b) μm from the original target surface. Time 0 represents the start of the heater pulses.

~ 100 μm from the target surface *are not* in agreement with the Thomson data [28]. However, it is well known that hydrodynamic simulations may have difficulties in properly calculating temperatures in the coronal region of the target. For examples see Refs. [18,32,33] which give an indication of the unresolved attempts to address the disagreement between simulated temperatures, used to generate spectra, and more direct observations.

As can clearly be seen from the above discussion, although we have independent information on the temperatures, we only have partial information on the densities, and there is still some reliance on hydrocode simulations. Evidently, improved density diagnosis (for example, by measuring both the electron and ion features in the Thomson scattering spectra) is desirable in future experiments.

In the discussion that follows we will concentrate on an analysis of the x-ray spectra observed at 50 and 300 μm from the original target surface. These two positions have been chosen for detailed study as the 50 μm distance represents the peak in the intensity of the emitted K-shell spectra, and 300 μm is the farthest position from the target surface at which we have confidence that the plasma expansion is one-dimensional, and at which we have Thomson scattering measurements. Furthermore, the analysis of the spectrum at this latter position is somewhat simplified by the fact that the plasma should essentially be optically thin to all but the strongest resonance-line radiation. Figures 2(a) and 2(b) show the time-resolved simulated electron density and the

measured electron temperatures for 50 and 300 μm from the original target surface, respectively. It is these parameters that were used to model the x-ray spectra using the atomic kinetics code, FLY.

IV. THE FLY ATOMIC PHYSICS CODE

In order to model the time integrated spectra the non-local-thermodynamic-equilibrium detailed-term atomic physics code FLY was used [34]. FLY is limited to calculation of only the primary emission lines in the spectra, though we would not expect to see significant inner-shell or satellite emission within the wavelength range (5.4–6.8 Å) covered by the time integrating SCS in such a long pulse experiment. FLY requires knowledge of the plasma atomic species Z, the ion and electron temperatures, and the electron density. A line-broadening function can also be included to account for any instrument or source broadening of the spectra.

FLY is a zero-dimensional code, however, the finite size of any real plasma can have a significant impact on the observed spectrum. Trapping of radiation due to the finite opacity of a particular line alters the atomic populations, while the effect of opacity on the radiation transfer must also be taken into account when calculating the observed spectrum along the direction from the plasma to a particular recording instrument. Although zero-dimensional in nature, the FLY code can take into account both of these effects in the following manner. The code essentially comprises two parts. In the first, the ionization and excitation populations are calculated for a given Z, ion and electron temperature, and electron (or ion) density. Within this calculation of the populations, the finite plasma size effects are incorporated by an "escape" distance, L_{esc}, which corresponds to the shortest distance that a photon needs to travel to escape from the plasma. This distance is then used to account for the effects of radiation trapping on the populations by means of the well-known escape-factor approximation.

In the second part of the calculation, the ionization and excitation populations are used to generate the synthetic spectrum. In this part of the calculation we input a second distance, L_{obs}, which corresponds to the effective thickness of the plasma as seen by the recording spectrometer. The code then uses this distance, in conjunction with the populations (and hence known opacities), to perform a simple radiation-transfer calculation along the line of sight to the recording instrument.

It is important to note that the two sizes, L_{esc} and L_{obs}, in the two separate portions of the calculation, can (and indeed, often should) be different: the pertinent distance for use in the population calculation will be the shortest distance that a photon needs to travel to escape the plasma, whilst the distance to be used in the subsequent calculation of the spectrum will be dictated by the angle of observation of the spectrometer with respect to the target, and the target dimensions. We will return to these matters in Sec. VII, where we discuss the comparison between the experimental and modeled x-ray spectra.
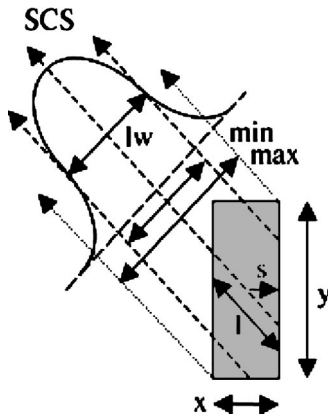
FIG. 3. Geometry of aluminum microdots: height $y = 200$ μm, width $x = 50\ 100\ 200$, or 400 μm; and as seen by the spectrometer: $l = L_{obs}$ the plasma depth, and lw the source broadened linewidths which must lie between min and max, see text. $s = L_{esc}$ is the shortest escape distance from the center of the plasma.

V. TARGET GEOMETRY AND SIZE

The single crystal spectrometer collected radiation from the aluminum plasma in a direction orthogonal to the plasma expansion, at an elevation angle of 45 ° to the orientation of the microdots, as shown in Fig. 3. The aluminum microdots were 200 μm high and varied as 50, 100, 200, or 400 μm in width. Given the low-dimensionality of the FLY code, it is therefore necessary to determine the appropriate values of L_{obs}, as defined in the previous section, for each of the target sizes. Consider the line of length l shown in Fig. 3. For emission that is optically thin, the appropriate value of L_{obs} will be $\sqrt{l^2}$, the rms of all possible chord lengths through the dot target. For the four target widths as listed above, L_{obs} by this definition is 60, 105, 163, and 210 μm, respectively. When using FLY to calculate the total number of photons that would be observed at the spectrometer, we clearly need to ensure that the number of photons seen will be proportional to the plasma volume in the optically thin limit. This is taken into account in the FLY calculations by means of an effective target width that ensures that L_{obs} multiplied by this width is equal to the known area of the dot. In this way the change with target size in the integrated line intensities per unit area as seen by the spectrometer can be directly related to changes in L_{obs}, the line of sight plasma depth. We will therefore present the *K*-shell spectral line intensities in units of photons cm^{-2} sr^{-1} mÅ^{-1}, and photons cm^{-2} sr^{-1} in the case of the integrated line-intensities, to highlight the effects of increasing the plasma depth, and also for ease of comparison with synthetically generated spectra or further experimental measurements.

Along with the effective thickness of the plasma along the line of sight, a further dimension of interest is the effective spatial width of the targets as seen by the single crystal spectrometer: the target source size is sufficient that all of the lines recorded by this spectrometer are source broadened. If we again consider optically thin emission, the FWHM of the spatial extent of the emission as seen by the spectrometer will be 140, 140, 140, and 280 μm respectively, denoted as

"min" in Fig. 3. The construction lines for this minimum linewidth intersect the top and bottom edges of the microdot at the midpoints, $x/2$, for all target widths. If we conversely consider the maximum possible spatial width of optically thick emission "max," the FWHM as seen by the spectrometer would be 176, 212, 282, and 424 μm respectively. When the effects of the finite slit width are taken into account the source sizes determined experimentally from the spectrum were 140, 155, 190, and 295 μm, respectively, these figures compare favorably with those expected from an optically thin plasma in most cases, but indicate that the effects of opacity cannot be completely neglected.

VI. SPECTRAL MODELING

FLY takes as its input L_{esc}, L_{obs}, Z, and the instrument broadening function. The time resolved electron temperatures, determined from the Thomson measurements, and the MEDUSA simulated densities, were then entered for the given distance of interest from the target surface. The ion temperature was assumed to be half the electron temperature. This was found from the hydrodynamic simulations to be a good approximation for all times of strong spectral emission.

By using the time-dependent measured electron temperatures and calculated densities from a given *position* in the plasma we are making the assumption that the atomic level populations depend only on these local conditions. Given the expanding nature of the plasma, a fully self-consistent calculation would require evolving in time the atomic populations for each Lagrangian *cell* of plasma, with the local hydrodynamic conditions encountered as it moves away from the target surface. The emission for a given position in the plasma could then be calculated from the populations of each cell that has crossed that particular point. However, as we have no measurements of the local temperature and density conditions between the target surface and 50 μm, such an analysis is problematic. However, given the relatively high electron densities in this region of the plasma, we believe that the local assumption should be fairly accurate for all the cases that we will consider.

Indeed, we can at least partially test this assumption for our two chosen positions of interest in the plasma, at 50 and 300 μm from the target surface. At 50 μm, where the simulated hydrodynamic conditions are in broad agreement with those measured, we can compare the full time-dependent ionization balance as calculated by MEDUSA to a steady-state calculation solely based on the local plasma conditions. The latter of these is achieved using the NIMP code [35] which is the same atomic physics package used to calculate the plasma ionization and excitation balance within the MEDUSA hydrocode. As Lagrangian cells within MEDUSA reach 50 μm away from the target surface, the hydrodynamic plasma conditions are extracted from the simulation and entered into NIMP. NIMP then calculates the steady-state solution to the ionization balance based on the local hydrodynamic conditions, to be compared to the full MEDUSA time-dependent solution at each time step. We find excellent agreement between these two solutions for the ionization balance at this point in the plasma. We therefore have confi-
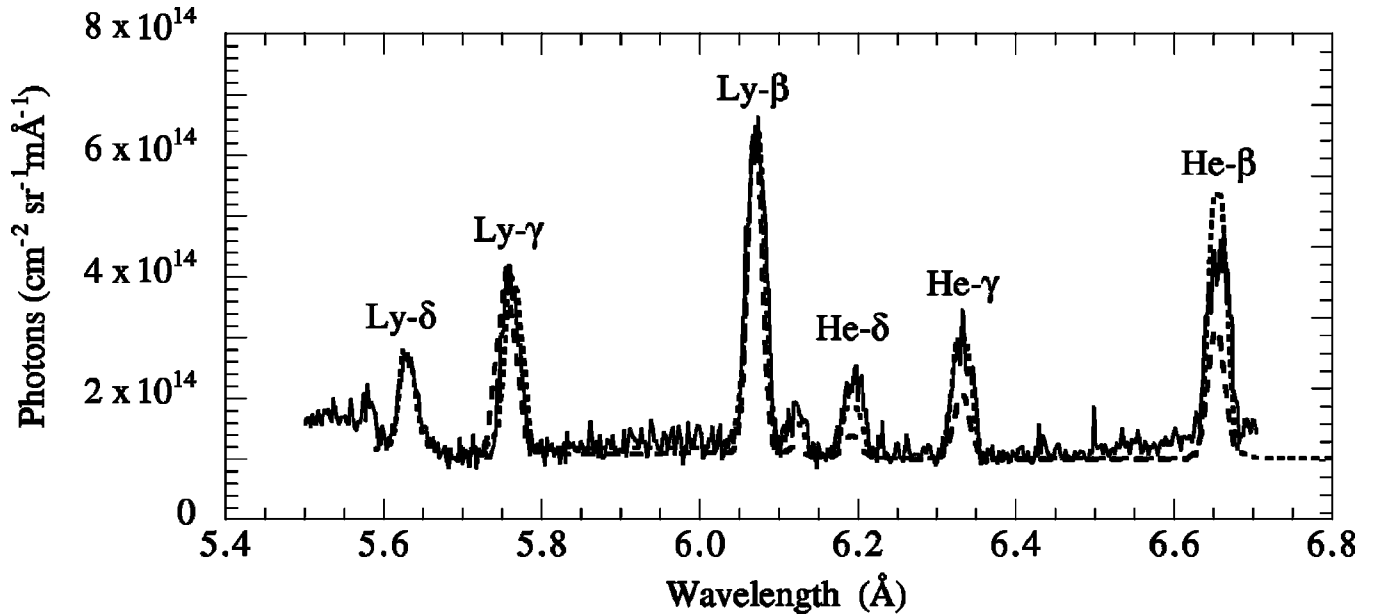
FIG. 4. Experimentally measured spectra at 300 μm from the target surface (solid line), compared with synthetic spectra generated from FLY with the ionization balance evolved time dependently (dotted) and in steady state (dashed) from the local plasma conditions.

dence that the steady-state assumption is valid for this region of the plasma, close to the target surface.

At 300 μm from the target surface it is not obvious that such a simple test should be valid. As we have previously stated in Sec. III and shown in Ref. [28], the temperatures produced by MEDUSA are considerably different from those measured in the experiment in this region of the plasma. A comparison of MEDUSA and NIMP at 300 μm from the target surface would therefore test whether the ionization balance for the simulated conditions was in steady state, but would not necessarily indicate whether this was also true for the experimental conditions. However, given that we are now confident that the conditions at 50 μm are indeed in steady state, we can use FLY to produce a set of time-dependent solutions for each plasma cell, starting from the conditions at 50 μm and ending at those measured at 300 μm. It should be recognized that this is by no means a completely valid solution as we do not know the full time history of the local plasma conditions between these two points. Generating spectra using FLY is also not currently practical using the temporally evolved conditions from 50 to 300 μm. We now compare the ionization and excitation balance produced by FLY for a steady-state solution, using the local temperature and density conditions at 300 μm, against those produced for a selection of plasma cells evolved time dependently from 50 to 300 μm. We find that until 0.2 ns after the laser has ceased there is no difference between the two solutions, beyond this time the steady-state solution overestimates the ionization, significantly reducing the heliumlike populations. This gives a strong indication that during the laser heater pulse and for 0.2 ns afterwards the plasma is indeed in steady state, but for later times time-dependent effects cannot be ignored.

A third solution can also be generated running FLY time dependently for the local temperature and density conditions

at 300 μm. At first this may seem a somewhat inconsistent calculation, as the ionization balance within a given plasma Lagrangian cell has no dependence on prior conditions at a given point, only on the prior conditions within the cell. However, while the plasma is in steady-state the time-dependent and steady-state solutions will be identical. For times beyond 0.2 ns after the heater pulse ends, when the plasma is no longer in steady state, it can be seen from Fig. 2(b) that the local electron temperature conditions are rapidly falling. It is also the case that the electron temperature within a given Lagrangian cell fall rapidly beyond this time. This is unsurprising given the heater pulses are no longer present and the expanding nature of the plasma. While using the local plasma conditions in a time-dependent ionization balance calculation is not strictly accurate, the general trends in the plasma hydrodynamic conditions are reproduced. Indeed, this solution produces a good agreement, with the ionization and excitation balance calculated by evolving the plasma cells time dependently from 50 to 300 μm, up to 0.7 ns after the heater pulse ceases. This local time-dependent solution also reduces the computing time necessary by a factor $\geq 10\,000$, compared to the more realistic case, and enables synthetic spectra to be generated for comparison with the experimental results.

At times beyond 0.2 ns after the heater pulses cease, when the plasma at 300 μm from the target surface is no longer in steady state, we are presently unable to perform a fully rigorous time-dependent calculation of the ionization balance. However, we have shown that a time-dependent solution, based on the local plasma conditions, produces a reasonable approximation up to 0.7 ns after the heater pulse ceases. This time span corresponds with the majority of emission of the K-shell spectral lines and hence we would still expect this solution, while not fully accurate, to approximately reproduce the measured emission spectra. It is hoped in the near

future that a more consistent solution will be possible using more sophisticated code calculations. In the following section we will comment on both the steady-state and the time-dependent FLY solutions in generating the emitted spectra from the local plasma conditions at 300 μm.

VII. K-SHELL SPECTRA: TIME-INTEGRATED DATA AND SIMULATIONS

We will start by looking at the spectral emission at 300 μm from the target surface. Using the four different size targets allows us to look at the differences in the absolute individual line intensities, as well as the intensity ratios between the lines, as the plasma length increases in the line of sight of the spectrometer. In this case we see that the line ratios between the six K-shell lines remain the same for all four targets, and that for each individual line the integrated intensity is directly proportional to the plasma depth, and hence the total photon count is proportional to the aluminum plasma volume. This indicates that the plasma is optically thin. Therefore to synthetically reproduce the line emission using FLY we take the optically thin approximation in the calculation of the atomic level populations. Figure 4 shows an experimentally measured spectrum for a 200 μm wide target compared with that produced from FLY, both evolving the ionization balance time dependently and in steady-state, using the local time-varying plasma conditions.

Excellent agreement is seen for the ratios between the three hydrogenic K-shell lines and both the time-dependent and steady-state FLY calculations. There is reasonable agreement for the three heliumlike lines with the time-dependent solution, but the steady-state solution produces a poor fit. Whilst the FLY spectra has been scaled to best fit the data there is in fact very good agreement in the absolute intensities to the hydrogenic series to better than $\pm 20\%$ for both FLY solutions, however, such good agreement is almost certainly slightly fortuitous as the experimental line intensities are only accurate to $\pm 50\%$, due to the level of uncertainty in the spectrometer throughput and the CCD detector efficiency. However, the relative line intensities are known to an accuracy of $\pm 10\%$ from the level of reproducibility of the experimental measurements. It is therefore the agreement between the data and FLY of the line ratios which provides the more useful information on the plasma conditions. Figure 5 shows the absolute intensities of the measured spectra against those predicted from FLY, both including and excluding the effects of opacity. Excellent agreement is found for all four targets for both the absolute line intensities and for the line ratios of the hydrogenic Lyman series lines. Given that the plasma is optically thin at this point, agreement with one target should automatically imply agreement with all target sizes. As we shall see in the following section for the case of 50 μm from the target surface, this agreement between the hydrogenic data and FLY is facilitated by the bulk of the emission being produced from early times when slowly changing hydrodynamic conditions validate the steady-state approximation.

However, for the heliumlike principle series lines a partial disagreement can be seen in both the line ratios and their
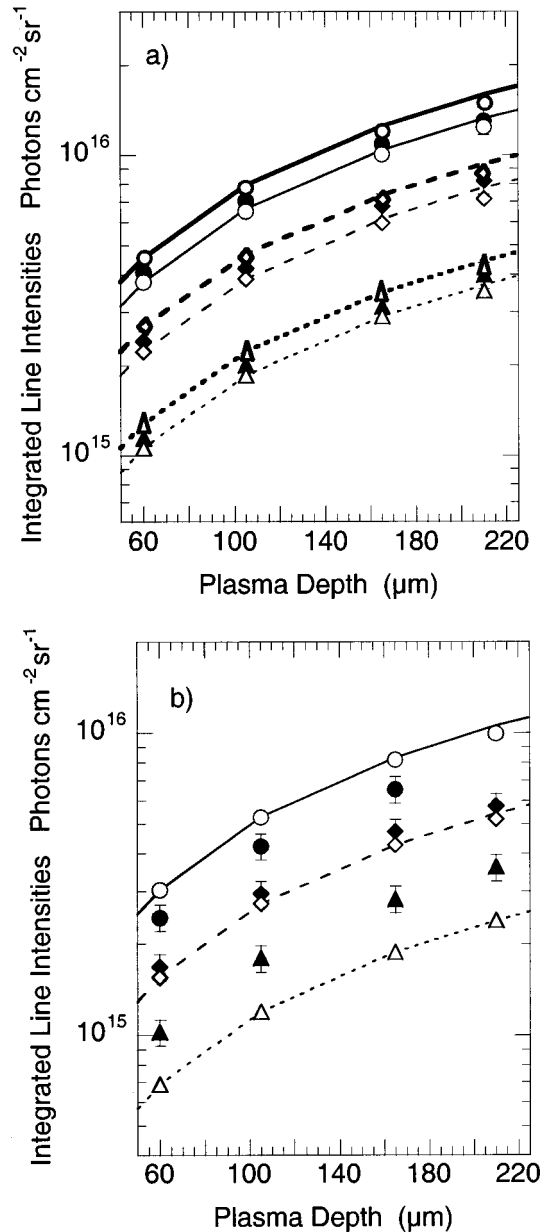

FIG. 5. Integrated K shell line intensities at 300 μm from the target surface as measured from the experiment (solid symbols), and as calculated using the local plasma conditions by FLY in steady state (bold) and time dependently (thin) including opacity (open symbols) and as optically thin (lines) for (a) the hydrogenic Lyman series, Ly-; (b) the heliumlike principle series, He-; β (circles, solid lines), γ (diamonds, dashed lines), and δ (triangles, dotted lines).

absolute intensities with the time-dependent FLY calculation. This disagreement almost certainly indicates the breakdown of the assumption of the ionization and excitation balance depending only on the local plasma conditions. Indeed, the steady-state FLY calculation shows integrated line intensities 50% less than those predicted in the time-dependent case (not shown in Fig. 5 for the sake of clarity). In the preceding section we noted that we have a good indication that this assumption is incorrect for late times when the density and temperature have significantly decreased from their peak values. It is not surprising, therefore, that it is the heliumlike
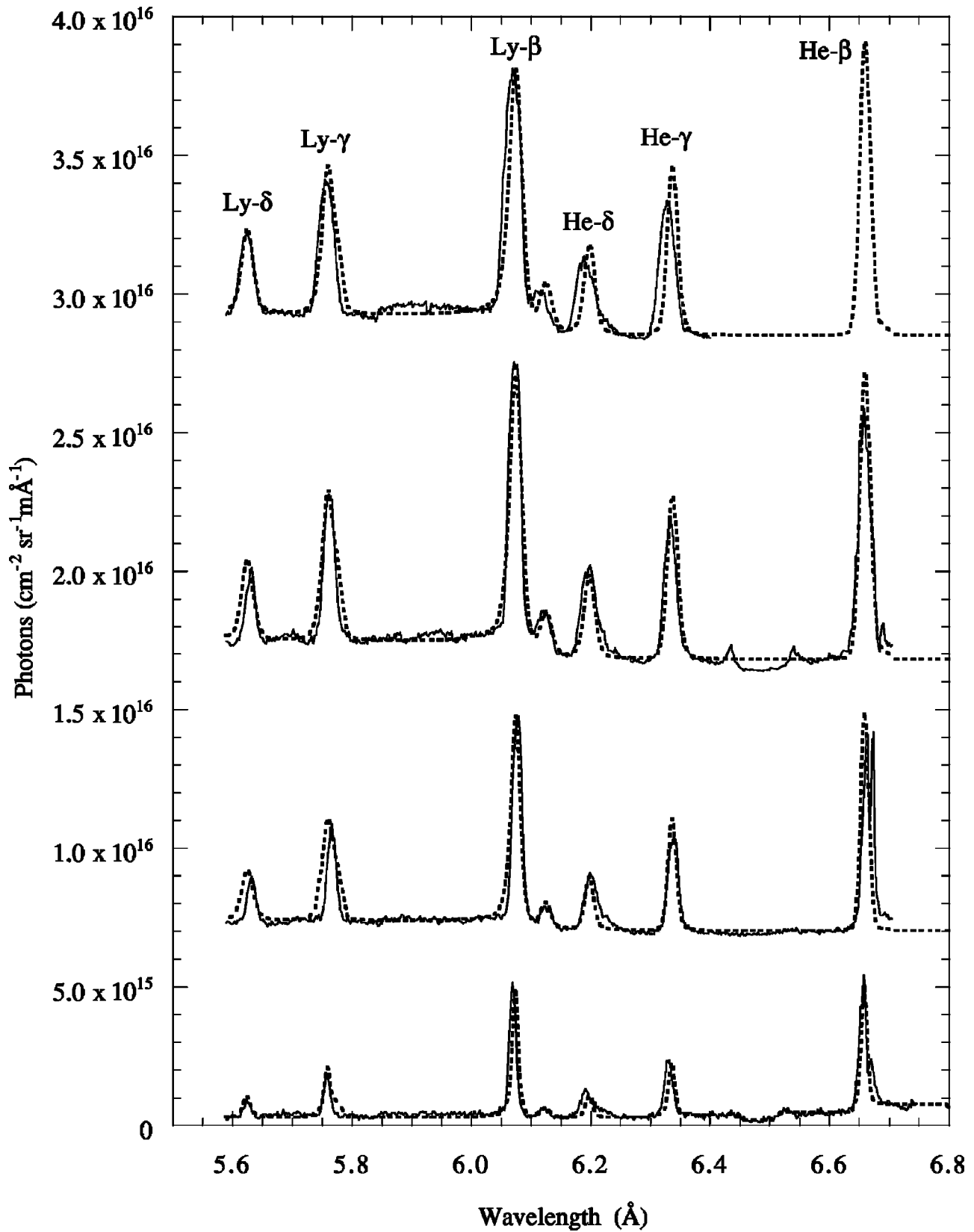
FIG. 6. Experimentally measured spectra (solid line) compared with synthetic spectra (dotted) generated from FLY for four width targets at the spatial peak of the spectral emission, 50 μm from the target surface. The spectra have been offset from each other for clarity, with the spectra from the 400 μm wide target ($+2.8\times10^{16}$ photons cm^{-2} sr^{-1} mÅ^{-1}) being at the top followed by that from 200 μm ($+1.6 \times10^{16}$), 100 μm ($+6.5\times10^{15}$) and with 50 μm (unshifted) at the bottom.

lines that are most affected by this; at the temperatures present at these late times we would expect heliumlike emission to dominate. Again we shall see this in more detail in the following section. It should also be noted that the absolute heliumlike line intensities should be underestimated by the FLY calculation as times beyond 2 ns are not considered, as we have no temperature measurements here. We would expect at least some heliumlike line emission beyond 2 ns, though we estimate this contribution to be $\leq 20\%$ of the individual line intensities. However, we would not expect any further hydrogenic line emission from these times. Taking this into account in the time integrated spectral intensities we find that the time-dependent FLY calculation overestimates the heliumlike contributions as compared to the hydrogenic emission by $\sim 10\%$, and the steady-state solution underestimates the overall helium emission by $\sim 40\%$. Whilst the time-dependent FLY calculation has produced a fairly good match to the spectral intensities, we would hope to use a fully self-consistent calculation in future, based on further time and space resolved temperature measurements.

At 50 μm from the target surface, the experimentally measured line ratios change with target width. This indicates that the plasma is not optically thin here, at least in the line of sight of the detector. In order to simulate the observed spectra we need to determine the appropriate escape distance, L_{esc}, to use in the calculation of the atomic populations. One might initially suppose that the plasma length that is of relevance, for including optical trapping in the calculation of the atomic level populations, is the shortest length from the center of the plasma to the edge [1], i.e., 25, 50, 100, and 100 μm, respectively (for the 400 μm wide target it is the 200 μm height which might be thought to provide the closest route for escape). However, in the case of a narrow atomic line and a steep velocity gradient, the direction of shortest escape can be along the plasma expansion direction, even though the total thickness of the plasma along this direction may be large. This is because in this expansion direction the emission profile of the line is Doppler shifted out of resonance with its own absorption profile in the faster moving ions further out into the plasma, as noted by Sobolev [36,37].

If we assume that the dominant local broadening mechanism is thermal Doppler broadening, then given the ion temperatures and velocity gradient from the hydrocode calculations, we deduce $L_{esc} \sim 10$ μm. Clearly the higher transitions, such as the Lyman γ and δ transitions will be Stark, rather than Doppler broadened. However, this should not affect the linewidths too dramatically, and we find that the excitation balance for $n \geq 4$ remains unchanged, at the level calculated as for optically thin ($L_{esc}=0$), up to values of $L_{esc} \leq 50$ μm.

Calculations based on the short escape distance of 10 μm, which is inferred from the high-velocity gradient, imply that the plasma is essentially optically thin to all line radiation in the plasma expansion direction. In practice, this will not be the case for the Ly-α line: this emission comprises the two fine structure components of the $2p_{3/2} \rightarrow 1s_{1/2}$ and $2p_{1/2} \rightarrow 1s_{1/2}$ lines. These lines are separated by only 5 mÅ, and the bulk Doppler shifts cause them to over-

lap, increasing the effective linewidth of the line, and greatly increasing the effective escape distance of the shorter wavelength component (full details of this mechanism can be found in Ref. [8]). At present, FLY has no means to take into account such effects, and thus for the present discussion we proceed assuming $L_{esc}=10$ μm. We find that the ionization and excitation balance calculation for such a short escape length is identical to taking the optically thin approximation $L_{esc}=0$. We will return to the possible implications of a higher opacity on the Ly-α transition in due course. The values of L_{obs} are taken to be those defined previously for each of the targets.

Figure 6 shows experimentally measured spectra from the four different width targets, at a distance of 50 μm from the target surface, compared with synthetic spectra generated from FLY using the values of L_{esc} and L_{obs} stated above. Excellent agreement is found for the ratios of the lines in all four spectra. A crystal defect can be seen at 6.5 Å, and this eventually prevented the He-β line from being measured on the 400 μm wide target shots. The line intensities are given in absolute photon numbers, with the brighter spectra being offset for clarity. We stress that the FLY synthetic spectra have been scaled to best fit each of the experimental line outs (we discuss the absolute photon numbers below). The excellent agreement for all the line ratios from the different width targets lends credence to the use of the optically thin approximation to the atomic level population calculation.

We note that the agreement for the line ratios and relative line intensities between the hydrogenic and heliumlike lines for 50 μm is now good, in contrast to the 300 μm spectra. This is no doubt due to the approximation, of the ionization and excitation balance being determined by the local plasma conditions only, being better suited to the higher density and temperature conditions closer to the target surface. Also we have temperature measurements for all times that the aluminum plasma is present at 50 μm, as the microdot fully ablates and moves beyond 50 μm in ~ 1.8–2 ns.

However, unlike the case of 300 μm from the target surface, the absolute intensities of the lines are not well reproduced by FLY. Figure 7 shows the line intensities for the six *K*-shell emission lines as a function of target size. Also shown are the intensities predicted by FLY, both including the effect of opacity in the line of sight and in the case of being optically thin. Indeed, the simulations can be seen to underestimate the line intensities in some cases by approximately a factor of 2. Also the experimentally measured individual line intensities do not scale as one might expect with plasma depth. Given that the optical depth along the line of sight to the spectrometer (i.e., L_{obs}) of the plasma increases with increasing target size, one might expect that the increase in the line intensities would be less than proportional to the plasma depth, the greater the optical depth of the line the smaller the expected increase. This effect can be seen by comparing the FLY calculations including and excluding the effects of opacity. If the data also behaved in this manner it would then be possible to calculate the optical depth of the plasma for each line, from the scaling of the line intensities with plasma depth. However, the measured line intensities can be seen to increase by a factor which is *larger* than the
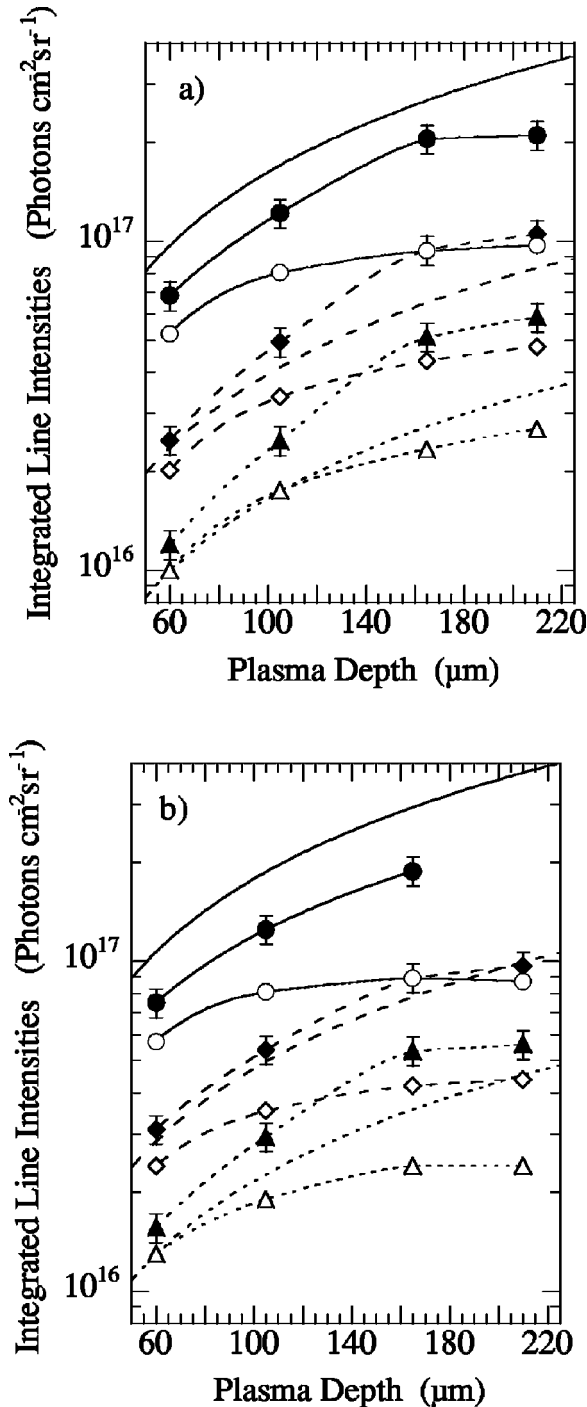
FIG. 7. Integrated K shell line intensities at 50 μm from the target surface as measured from the experiment (solid symbols), and as calculated using the local plasma conditions by FLY in steady state, including opacity (open symbols and lines) and as optically thin (lines with no symbols) for (a) the hydrogenic Lyman series, (b) the heliumlike principle series. Symbols are as in Fig. 5.

increase in plasma depth, except in the largest target case. This is, therefore, an intensity scaling over and above that expected even for an optically thin plasma. This increase is largest for the δ lines and smallest for the β lines; indeed the β lines scale almost as the target size.

A possible explanation for this increased scaling can be

found by looking again at the calculation of the atomic level populations, and at the optically thin approximation. Whilst the optically thin approximation was valid for the β, γ, and δ transitions, as noted it may well not be the case for the α transitions. The measurements of Ly-α from the DCV and the SCS show that the measured line intensity is 50 times that calculated by FLY using the optically thin populations. The α transitions have a much greater line strength and as such have a greater optical depth for a similar plasma length than the higher n transitions. Also, whereas the velocity gradient facilitated the escape of the higher n transition lines in the plasma expansion direction, for the Ly-α lines this will lead to overlapping of the lines and hence a greatly increased value of L_{esc} in this direction. This greater depth leads to population trapping on the $n=2$ level, greatly increasing the population over that of the optically thin case. Such trapping will, in turn, have an influence on the intensity of each of the higher n transitions.

If L_{esc} becomes sufficiently large in the plasma expansion direction, then the relevant value of L_{esc} for calculation of the $n=2$ populations becomes the shortest distance from the center to the edge of the plasma, which is 25, 50, 100, and 100 μm for each target size, respectively, as noted previously. This could then explain the increased intensity scaling of the K-shell lines between the three smaller target sizes, and the reduced scaling to the largest target size, as the level of population trapping on the $n=2$ level would be determined by these values of L_{esc}. Indeed, simulations with FLY using a longer value of L_{esc} show an increase in the $n=2$ populations, and the intensities of the higher n transitions as expected, though the line ratios are now not matched. As noted above, the close proximity of the two fine structure components to each other invalidates the use of the single escape distance employed within FLY.

Whilst the ability of FLY to reproduce correctly the line ratios for all four target thicknesses is impressive, the difficulties in obtaining the correct photon numbers may be some indication of the limitations of using such a low-dimensional model to analyze what is essentially a three-dimensional problem. We return to this point in the discussion in Sec. X. The excellent match to all of the line ratios of the measured spectra by the FLY synthetic spectra when relying on temperature and densities from independent measurements is extremely encouraging.

VIII. K-SHELL SPECTRA: TEMPORAL EVOLUTION

It is also of interest to look at the predicted timing of the emission relative to the hydrodynamic evolution of the plasma. Figure 8 shows the time integrated synthetic spectra from FLY for 0–1 ns (solid line) and for 1–2 ns (dotted line) at 50 μm from the target surface, where 0 and 1 ns represent the beginning and end of the laser heater pulses, respectively. The MEDUSA simulations predict that the aluminum microdot would have been completely ablated and the aluminum plasma moved beyond 50 μm from the target surface at times beyond 2 ns, though this time is extremely sensitive to target thickness. 2 ns also represents the latest time at which we have electron temperature measurements from Thomson
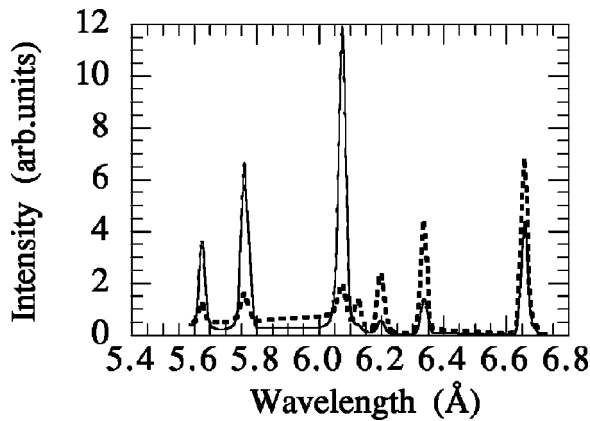
FIG. 8. Synthetic spectra integrated for during (solid) and after (dotted) the heater pulses.
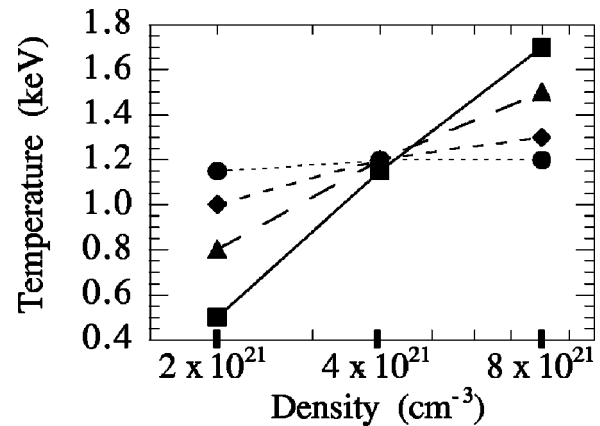

FIG. 9. Electron densities and temperatures at which the FLY synthetic spectra match the experimentally measured hydrogenic Lyman series emission lines for the four different width targets, 400 μm wide target (squares), 200 μm (triangles), 100 μm (diamonds), and 50 μm (circles).

scattering. It is clear that the hydrogenic and the heliumlike aluminum principle series are emitted at different times during the plasma, and hence derive from differing hydrodynamic conditions. This highlights the importance of using the temporally evolving hydrodynamic parameters, and the inherent dangers of associating a single temperature or density, from time integrated spectra, based on line ratios between different ion stages.

There is significant heliumlike aluminum line emission during the entire 2 ns time period, but with a bias towards stronger emission at times after the heater beams are turned off. From Fig. 2 it is clear that the plasma has considerably cooled at these times. Indeed the peak in the heliumlike emission is found to occur at electron temperatures of 300–400 eV between 400 and 700 ps after the heater beams are turned off. In contrast, the hydrogenic Lyman series of emission lines can be seen to be almost exclusively emitted in the first 1 ns, while the heater beams are still focused onto the target. In fact, 87% of the hydrogenic Lyman series is emitted during the time period when the heater pulses are on, indicating an electron temperature of between 1.1 and 1.3 keV, significantly in excess of the temperature that dominates during the heliumlike emission. The fact that whilst the hydrogenic emission is being generated the hydrodynamic parameters change little, provides an opportunity to study these lines without the constraints of their temporal evolution.

Figure 9 shows the results of an attempt to synthetically reproduce the hydrogenic Lyman series emission line ratios using a single electron temperature and density, steady-state FLY solution. We again use $L_{esc} = 10$ μm for calculating the atomic level populations and the appropriate values of L_{obs} discussed previously. The points at which the FLY spectral line-ratios best match the measurements are marked for each of the four different width targets. In each target width case a match can be found to an accuracy of better than 5%. The synthetic spectra are essentially the same for changes in the electron temperature of ± 50 eV, and electron density of $\pm 5 \times 10^{20}$ cm^{-3}. Two points are immediately obvious from this analysis: that a single electron temperature-density solution exists for all target widths, at 1.2(± 0.1) keV and 4 (± 1) $\times 10^{21}$ cm^{-3}, and that there are multiple other solutions outside these bounds for each individual target width.

Shown are solutions at electron densities of 2, 4 and 8 $\times 10^{21}$ cm^{-3}, but solutions exist for some targets between 5×10^{20} and 2×10^{22} cm^{-3}, beyond this range no sensible matches (within $\pm 20\%$) can be found. An analysis, independent of further hydrodynamic information, is therefore only possible due to the multiple target widths. For a single width target there must be prior knowledge of either the electron temperature or density for the other to be calculated, even for this simplified case of a homogeneous plasma. Given this single solution we can compare these electron temperatures and densities with those during the heater pulses from the time-dependent solution shown in Fig. 2. The single electron temperature of 1.2(± 0.1) keV covers the range of temperatures present during the heater pulses. The single density of 4(± 1) $\times 10^{21}$ cm^{-3}, is also in excellent agreement with that simulated for the time period whilst the heater pulses are on.

Figure 10 shows the measured experimental time integrated hydrogenic Lyman series emission lines, compared with the unique synthetic steady-state solution of FLY for the single electron temperature and density found above. The match is seen to be excellent again for all four target widths.

Figure 11 shows the change in the line ratios between Ly-γ and Ly-β, Ly-δ, and Ly-β, and Ly-δ and Ly-γ as the target width is increased as measured in the experiment, and from the unique single temperature-density FLY solution. A significant change can be seen from the thinnest to the thickest targets for all the ratios, indicating the increasing effect of opacity with increasing plasma width. The greatest changes can be seen in the ratios between Ly-β and the higher *n* transitions, whereas there is a smaller relative change in the Ly-δ to Ly-γ ratio with increasing plasma depth. This is indicative of the greater relative optical depth of the Ly-β transition, and that the Ly-δ transition must be very close if not actually optically thin in all cases. FLY calculations for an optically thin plasma yield Lyman line ratios very similar to those seen for the case of the 50 μm wide target. This is a good indication that for the narrowest width target the plasma is approximately optically thin and that the line ra-
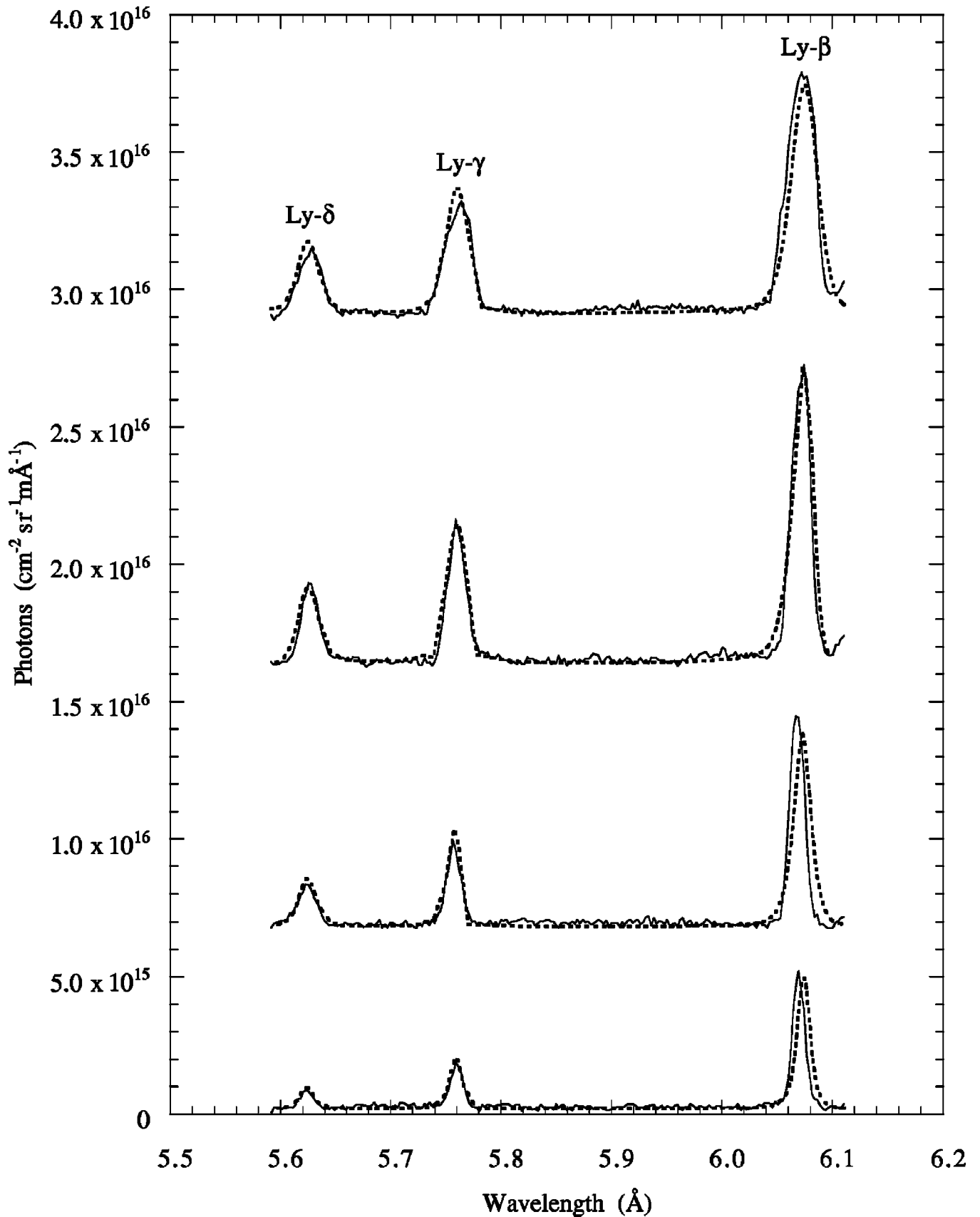
FIG. 10. Experimental (solid line) and synthetic hydrogenic Lyman series spectra (dotted) for a single electron temperature and density of 1.2 keV and 3×10^{21} cm^{-3}. The spectra from the four different width targets have been spatially separated for clarity, see Fig. 6 for details.
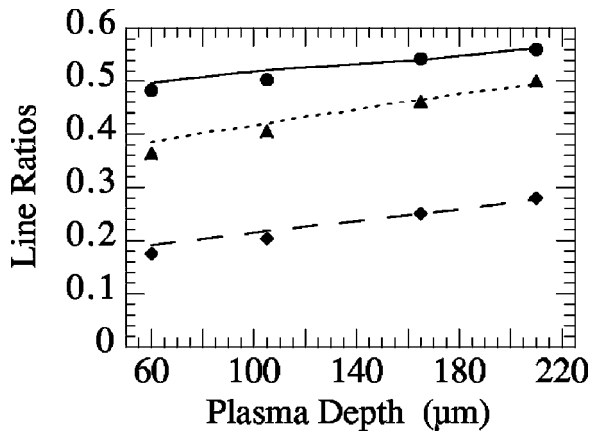
FIG. 11. Effect of increasing the target width on the experimentally measured hydrogenic Lyman line ratios (points) against those calculated by FLY [lines] using a single electron temperature and density, Ly-δ/Ly-β (diamonds) [dotted line], Ly-γ/Ly-β (triangles) [dashed], Ly-δ/Ly-γ (circles) [solid].

diation escapes without further interaction with the plasma in the direction of the spectrometer. This is further verified by Fig. 9, where the good agreement, between the measured spectra from the 50 μm wide target and that calculated from FLY, is insensitive to the electron density.

IX. *K*-SHELL SPECTRA: LINEWIDTHS

All indications show that the hydrogenic Lyman series lines were emitted during a time frame when the electron temperatures and densities were approximately constant. It is therefore possible to verify the electron density using the line widths measured at high spectral resolution by the VJS. Note that in all the experimental and synthetic spectra produced thus far the spectral width of the lines have been determined by source broadening. The high dispersion of the VJS renders source broadening negligible, and thus the recorded linewidths of the high n transitions will be determined by Stark broadening. The targets used for these measurements were 100×100 μm square and 1 μm thick, and the spectrometer viewed side on to the targets. Figure 12 shows the comparison between the experimentally measured line profiles for Ly-β and Ly-δ and those synthetically generated from FLY, for 20, 50, and 100 μm from the original target surface. At a distance of 50 μm from the target surface, excellent agreement is found with an electron temperature of 1.2 keV and an electron density of $3(\pm 1) \times 10^{21}$ cm^{-3}. This density inferred from the Stark width of the line is in excellent agreement with the electron densities inferred from the time-integrated data in Secs. VII and VIII. It should be noted that changing the electron temperature in the FLY calculations between 1 and 2 keV has no effect on the calculated linewidths.

Figure 13 shows the MEDUSA calculated electron density for times of 0.3, 0.6, and 1.0 ns after the start of the heater pulse. Further, we show in Fig. 13 the densities at which the FLY line profiles agree with those recorded experimentally. At 20 μm there is a slight discrepancy between the density inferred from the Ly-β and Ly-δ line-profiles. This could
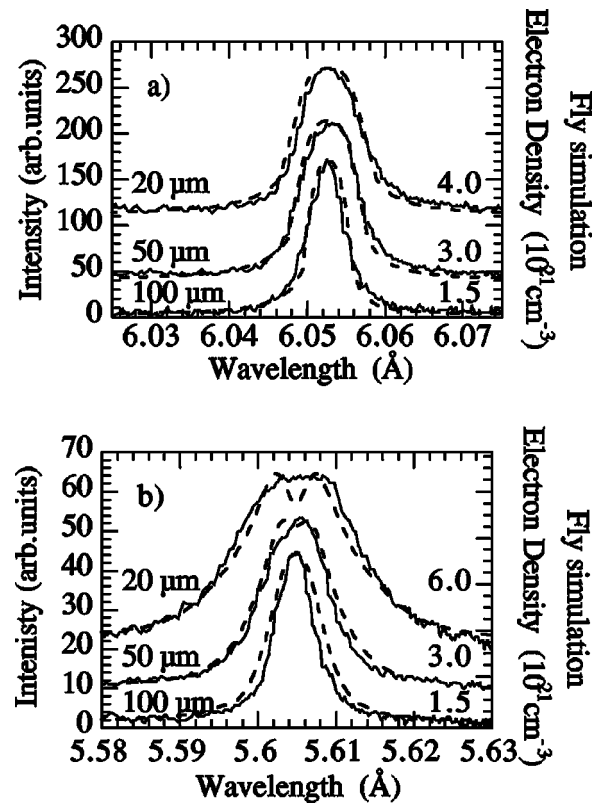

FIG. 12. Line profiles for observed Ly-β (12a) and Ly-δ (12b) emission lines (solid line) against FLY synthetic profiles (dotted) for different distances away from the target surface. The spectra at 20, 50 and 100-μm are shown, offset for clarity, and the electron densities corresponding to the best fit from FLY are given.

indicate that the lines have been preferentially emitted at different times during the heater pulses, as at 20 μm the density can be seen to fall slightly with time. However, if this were the case we would expect this difference to also show up at 100 μm where the temporal variation in density is larger. A more credible explanation is that at these higher densities the calculations of FLY are starting to become less reliable as the ionization balance is affected by the emitted radiation. If this is the case the Ly-δ width should provide a more accurate density measurement, as it will be less optically thick. At distances beyond 100 μm the temporal variation in the electron density becomes more substantial, so that a unique electron density measurement has less meaning. Also, at densities below 1×10^{21} cm^{-3} the FLY calculated widths are much less density sensitive, and indeed the measured line profiles show a constant width from 150 μm outwards, indicating that they are no longer dominated by Stark broadening.

Figure 14 shows that the Ly-β width calculation also provides a separate measurement of the effects of opacity on the line profiles. The width of the Ly-β profile is sensitive to opacity, whereas the Ly-δ profile is effectively optically thin at a target plasma depth of 100 μm. This provides further evidence that it is most likely the opacity effect on the width of the Ly-β line that creates the discrepancy between the electron density fits at 20 μm. There is still excellent agree-
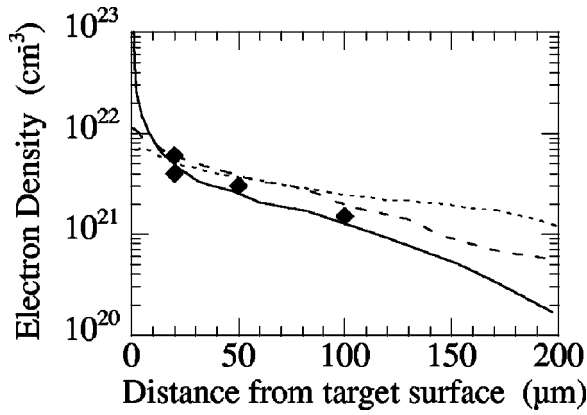
FIG. 13. Simulated electron densities from MEDUSA at 0.3 (solid line), 0.6 (dashed), and 1.0 ns (dotted) after the start of the heater pulses. The diamonds represents the positions and densities at which the FLY synthetic line profiles match those of the experimental spectra for Ly-β or Ly-δ.

FIG. 14. Synthetic line profiles from FLY with (solid line) and without (dotted) the effects of opacity included; for Ly-β (right) and Ly-δ (left).

ment for both line profiles at the simulated electron densities, showing the accuracy of the FLY spectral width calculation.

The level of consistency in these measurements is exceptional, leading us to have a high level of confidence in the accuracy of these measurements. This consistency also shows the ability of FLY to reproduce the ionization and excitation balance of the hydrogenic aluminum plasma, and to accurately synthesize the emitted spectra, incorporating the effects of opacity in the line ratios and line profiles.

X. SUMMARY AND CONCLUSIONS

In this paper we have presented electron temperature measurements and electron density simulations for a laser-produced uniaxially expanding aluminum plasma. The electron density simulations have been shown to be consistent with shadowgram images at low density [28], and are shown to be accurate at high density through Ly-β and Ly-δ line-width measurements. Independent temperature measurements were made by means of Thomson scattering. Using these time-dependent hydrodynamic conditions as input to the non-LTE detailed term atomic physics code FLY, the ratios of the lines in the experimentally measured K-shell spectra are reproduced to a high degree of accuracy. This high level of agreement strengthens the validity of the assumption that the atomic level populations are given solely by the local time-dependent thermodynamic conditions.

Four different size aluminum microdot targets were used and the plasma conditions analyzed at two different positions from the target surface. At distances far from the target surface the direct intensity scaling of the individual K-shell lines with the target size shows that the plasma is optically thin. This is confirmed by the agreement with the synthetic FLY hydrogenic spectra, in both the absolute line intensities and the line ratios, using the optically thin approximation for the calculation of the atomic populations and of the radiation transfer through the plasma. The agreement with the FLY heliumlike spectra is not as good, and this was shown to be an indication of the breakdown of the steady-state approxima-
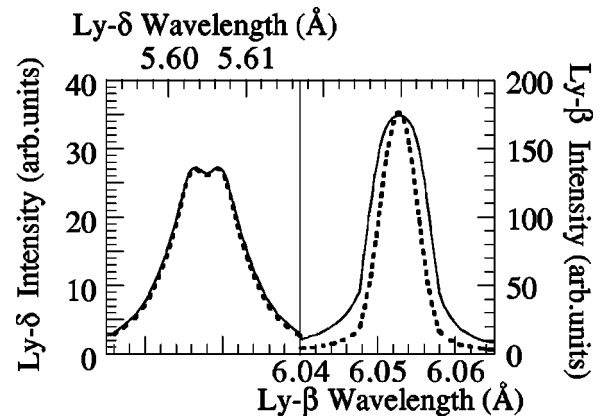
tion at late times when the heliumlike emission is expected to dominate. While a time-dependent FLY calculation, based on local plasma conditions, produced a reasonable approximation to the late-time ionization balance and to the emitted heliumlike spectra, it is hoped in future to use a more consistent calculation based on further time-dependent hydrodynamic measurements.

At higher densities closer to the target surface the K-shell line ratios show the effects of optical depth with increasing target size. However, careful analysis of the plasma expansion shows that for the emission lines under consideration the populations are well matched by a simulation where the escape distance of the photons is determined by the steep nature of the velocity gradient in the plasma expansion direction. It is mainly in the line of sight of the spectrometer and hence in the radiation transfer that the effects of opacity must be considered. Again the excellent agreement with the ratios of the lines in the FLY synthetic spectra for all size targets validates the approximations made, and the ability of FLY to take into account optical depth in the radiation transfer.

Both the FLY and MEDUSA calculations show that the peak of the hydrogenic Lyman series of emission lines should be emitted during a time interval where the hydrodynamic parameters are nominally constant. Indeed, a fit to the hydrogenic Lyman series line ratios for all the targets can be found using a single temperature and density in FLY of 1.2 (± 0.1) keV and $4(\pm 1) \times 10^{21}$ cm^{-3}. For the heliumlike emission series no such steady-state solution exists, as significant emission occurs for a large variety of electron temperatures and densities. The peak of the heliumlike principle series emission occurs later in time than that of the hydrogenic series, and at lower electron temperatures of 300–400 eV. This highlights the danger of associating a single electron temperature from line ratios between different ionization stages in a laser-produced plasma. Moreover, FLY can synthetically reproduce the hydrogenic Lyman series spectra from a single width target with a range of combinations of electron temperatures and densities. However, there is only one combination which produces a match for all four different target widths. For experiments with only one size of tar-

get, independent knowledge of one of the hydrodynamic parameters would therefore be necessary to calculate the other from the measured spectra.

However, whilst the line ratios are well matched, it was shown that at 50 μm from the target surface, where the density is higher, the absolute intensities of the lines differed from those simulated by up to a factor of 2. Also, the intensity scaling of the *K*-shell emission lines with increasing target size was over and above that expected even for optically thin targets. One possible explanation put forward was the difference in the escape length that should be used for the Ly-α radiation compared with that actually used. Increased optical trapping could well alter the $n=2$ populations, and therefore the populations of the higher lying states. Indeed, this slight inconsistency highlights the difficulties in using a zero-dimensional code such as FLY to model what is essentially a three-dimensional problem. Associating a unique length with photon escape is clearly a highly-idealized approximation. It would be of great interest to attempt to model the experimental data presented here with a more sophisticated radiation-transfer simulation that can either use escape factors with high dimensionality, and/or perform a self-consistent calculation of the radiation field and atomic populations, and take into account the inhomogeneity of the plasma. Codes with this degree of complexity do exist (for example the CRETIN code [38]), and we aim to present the results of such an analysis in a future publication. It is certainly of interest to explore whether experimental data can be recorded with sufficient resolution and accuracy so as to be sensitive to the degrees of complexity within such codes.

Further improvements to experiments could be made to obtain a set of data that could be used to provide benchmark data for simulations. First, it is important to have more extensive information on the temporal evolution of the electron density at positions closer to the target surface. Such measurements could be made by extending the Thomson scattering diagnostic to include the recording of the electron feature, and/or by use of interferometry.

Furthermore, we are now in a position to begin to analyze the effect of the velocity gradient on the line shape of the Ly-α emission. This will provide a further test of the atomic kinetics code used, as we have shown that the plasma opacity cannot be ignored in the ionization balance calculations. The doublet nature of this transition will play an important role in the ionization balance calculation, as the velocity gradient will ensure absorption of the emission from one line by the other in separate parts of the plasma. This will also greatly affect the spectral line shape, which can be resolved by the DCV spectrometers. These measurements, along with the known hydrodynamic conditions, should therefore provide a further test for more sophisticated radiation transport calculations.

[1] D. Mihalas, *Stellar Atmospheres* (Freeman, San Francisco, 1978).

[2] R. W. Lee, J. Quant. Spectrosc. Radiat. Transf. **27**, 87 (1981).

[3] D. G. Hummer and G. B. Rybicki, Astrophys. J. **254**, 767 (1982).

[4] G. B. Rybicki, *Methods in Radiative Transfer* (Cambridge University Press, New York, 1984).

[5] D. C. Eder and H. A. Scott, J. Quant. Spectrosc. Radiat. Transf. **45**, 189 (1991).

[6] J. S. Wark, A. Djaoui, S. J. Rose, H. He, O. Renner, T. Missalla, and E. Foerster, Phys. Rev. Lett. **72**, 1826 (1994).

[7] J. S. Wark, H. He, O. Renner, M. Kopecky, E. Foerster, and T. Missalla, J. Quant. Spectrosc. Radiat. Transf. **51**, 397 (1994).

[8] P. K. Patel, J. S. Wark, D. J. Heading, A. Djaoui, S. J. Rose, O. Renner, and A. Hauer, J. Quant. Spectrosc. Radiat. Transf. **57**, 683 (1997).

[9] P. K. Patel, J. S. Wark, O. Renner, A. Djaoui, S. J. Rose, D. J. Heading, and A. Hauer, J. Quant. Spectrosc. Radiat. Transf. **58**, 835 (1997).

[10] P. K. Patel, E. Wolfrum, O. Renner, A. Loveridge, R. Allott, D. Neely, S. J. Rose, and J. S. Wark, J. Quant. Spectrosc. Radiat. Transf. **65**, 429 (2000).

[11] O. Renner, M. Kopecky, J. S. Wark, H. He, and E. Foerster, Rev. Sci. Instrum. **66**, 3234 (1995).

[12] O. Renner, T. Missalla, P. Sondhauss, E. Krousky, E. Foerster, C. Chenais-Popovics, and O. Rancu, Rev. Sci. Instrum. **68**, 2393 (1997).

[13] M. H. Key, C. L. S. Lewis, J. G. Lunney, A. Moore, J. M. Ward, and R. K. Thareja, Phys. Rev. Lett. **44**, 1669 (1980).

[14] P. Audebert, J. P. Geindre, J. C. Gauthier, and C. Popovics, Phys. Rev. A **30**, 768 (1984).

[15] P. Alaterre, C. Chenais-Popovics, P. Audebert, J. P. Geindre, and J. C. Gauthier, Phys. Rev. A **32**, 324 (1985).

[16] J. P. Apruzese, D. Dunston, and J. Davis, J. Quant. Spectrosc. Radiat. Transf. **36**, 339 (1986).

[17] W. H. Goldstein, R. S. Walling, J. Bailey, M. H. Chen, R. Fortner, M. Klapisch, T. Philips, and R. E. Stewart, Phys. Rev. Lett. **58**, 2300 (1987).

[18] R. L. Kauffman, R. W. Lee, and K. G. Estabrooa, Phys. Rev. A **35**, 4286 (1987).

[19] B. K. F. Young, R. E. Stewart, C. J. Cerjan, G. Charatis, and G. E. Busch, Phys. Rev. Lett. **61**, 2851 (1988).

[20] R. S. Marjoribanks, M. C. Richardson, P. A. Jaanimagi, and R. Epstein, Phys. Rev. A **46**, R1747 (1992).

[21] S. H. Glenzer, C. A. Back, K. G. Estabrook, B. J. MacGowan, D. S. Montgomery, R. K. Kirkwood, J. D. Moody, D. H. Munro, and G. F. Stone, Phys. Rev. E **55**, 927 (1997).

[22] L. Aschke, S. Depierreux, K. G. Estabrook, K. B. Fournier, J. Fuchs, S. H. Glenzer, R. W. Lee, W. Rozmus, R. S. Thoe, and P. E. Young, J. Quant. Spectrosc. Radiat. Transf. **65**, 23 (2000).

[23] S. H. Glenzer, K. G. Estabrook, R. W. Lee, B. J. MacGowan, and W. Rozmus, J. Quant. Spectrosc. Radiat. Transf. **65**, 253 (2000).

[24] S. H. Glenzer, K. B. Fournier, C. Decker, B. A. Hammel, R. W. Lee, L. Lours, B. J. MacGowan, and A. L. Osterheld, Phys. Rev. E **62**, 2728 (2000).

[25] D. E. Evans and J. Katzenstein, Rep. Prog. Phys. **32**, 207 (1969).

[26] S. H. Glenzer *et al.*, Phys. Plasmas **6**, 2117 (1999).

[27] I. N. Ross, M. S. White, J. E. Boon, D. Craddock, A. R. Damerell, R. J. Day, A. F. Gibson, P. Gottfeldt, D. J. Nicholas, and C. Reason, IEEE J. Quantum Electron. **17**, 1653 (1981).

[28] D. M. Chambers *et al.*, J. Quant. Spectrosc. Radiat. Transf. **71**, 237 (2001).

[29] J. Hawreliak *et al.*, J. Quant. Spectrosc. Radiat. Transf. **71**, 383 (2001).

[30] J. P. Christiansen, D. E. T. F. Ashby, and K. V. Roberts, Comput. Phys. Commun. **7**, 271 (1973).

[31] A. Djaoui and S. J. Rose, J. Phys. B **25**, 2745 (1992).

[32] R. W. Lee and K. G. Estabrook, Phys. Rev. A **35**, 1269 (1987).

[33] B. K. F. Young, W. H. Goldstein, A. L. Osterheld, R. E. Stewart, G. Charatis, and G. E. Busch, J. Phys. B **22**, L533 (1989).

[34] R. W. Lee and J. T. Larsen, J. Quant. Spectrosc. Radiat. Transf. **56**, 535 (1996).

[35] S. J. Rose, Rutherford Appleton Laboratory Technical Report No. RAL–TR–97–020, 1997 (unpublished).

[36] V. V. Sobolev, Sov. J. of Astron. Astrophys. **1**, 678 (1957).

[37] V. V. Sobolev, *Moving Envelopes of Stars* (Harvard University Press, Cambridge, 1960).

[38] H. A. Scott, J. Quant. Spectrosc. Radiat. Transf. **71**, 689 (2001).